MARTIN MARIETTA ENERGY SYSTEMS LIBRARIES

3 4456 0056841 9

ORNL/TM-9685

ornl

OAK RIDGE NATIONAL LABORATORY

MARTIN MARIETTA

Magnetic Field Alignment Studies for the URAGAN-3 Torsatron

R. J. Colchin
S. I. Fedotov
J. H. Harris
D. K. Lee
F. I. Ozherel'ev
O. S. Pavlichenko
D. P. Pogozhev
J. A. Rome
J. D. Treffert
V. M. Zalkind

OAK RIDGE NATIONAL LABORATORY
CENTRAL RESEARCH LIBRARY
CIRCULATION SECTION
4500N ROOM
LIBRARY LOAN COPY
DO NOT TRANSFER TO ANOTHER PERSON
If you wish someone else to see this report, send in name with report and the library will arrange a loan.

OPERATED BY
MARTIN MARIETTA ENERGY SYSTEMS, INC.
FOR THE UNITED STATES
DEPARTMENT OF ENERGY

Printed in the United States of America. Available from
National Technical Information Service
U.S. Department of Commerce
5285 Port Royal Road, Springfield, Virginia 22161
NTIS price codes—Printed Copy: A03, Microfiche A01

This report was prepared as an account of work sponsored by an agency of the United States Government. Neither the United States Government nor any agency thereof, nor any of their employees, makes any warranty, express or implied, or assumes any legal liability or responsibility for the accuracy, completeness, or usefulness of any information, apparatus, product, or process disclosed, or represents that its use would not infringe privately owned rights. Reference herein to any specific commercial product, process, or service by trade name, trademark, manufacturer, or otherwise, does not necessarily constitute or imply its endorsement, recommendation, or favoring by the United States Government or any agency thereof. The views and opinions of authors expressed herein do not necessarily state or reflect those of the United States Government or any agency thereof.

ORNL/TM-9685
Dist. Category UC-20

Fusion Energy Division

MAGNETIC FIELD ALIGNMENT STUDIES FOR THE URAGAN-3 TORSATRON

R. J. Colchin
S. I. Fedotov*
J. H. Harris
D. K. Lee+
F. I. Ozherel'ev*
O. S. Pavlichenko*
D. P. Pogozhev*
J. A. Rome
J. D. Treffert≠
V. M. Zalkind*

*Kharkov Physico-Technical Institute, Kharkov, U.S.S.R.
+Computing and Telecommunications Division, Martin Marietta Energy Systems, Inc.
≠Torsatron/Stellarator Laboratory, University of Wisconsin, Madison.

Date Published - February 1986

Prepared by the
OAK RIDGE NATIONAL LABORATORY
Oak Ridge, Tennessee 37831
operated by
MARTIN MARIETTA ENERGY SYSTEMS, INC.
for the
U.S. DEPARTMENT OF ENERGY
under Contract No. DE-AC05-84OR21400

MARTIN MARIETTA ENERGY SYSTEMS LIBRARIES
3 4456 0056841 9

CONTENTS

ABSTRACT..... v

I. INTRODUCTION..... 1

II. CALCULATED FLUX SURFACES IN URAGAN-3..... 3

III. MAGNETIC FIELD MEASUREMENTS..... 6

A. Procedure..... 6

B. Apparatus..... 7

C. Overall Magnetic Field System Tests..... 8

D. Separate Determination of the VF and Helical Coil Axes.... 12

1. Axis of the VF Coils..... 12

2. Axis of the Helical Coils..... 16

3. Axis of the VF Coils After Realignment..... 18

IV. DISCUSSION OF RESULTS..... 21

ACKNOWLEDGMENTS..... 25

REFERENCES..... 26

ABSTRACT

If the major axes of the helical and vertical field coils of a torsatron plasma confinement device are not aligned to within ~1% of their major radii, the resulting error field can break up closed magnetic flux surfaces and reduce the effective plasma confinement volume. A novel technique for accurately locating the magnetic symmetry axes of torsatron helical and vertical coil sets to within ~1 mm using magnetic field measurements near the device major axis (i.e., away from the confinement volume) is described and applied to the URAGAN-3 torsatron. The axis of the vertical field coil set was found to be shifted by ~1 cm relative to the axis of the helical coil set; this shift could account for the reduced confinement volume observed in previous experiments. The magnetic measurements were repeated after coil repositioning to verify correct alignment.

I. INTRODUCTION

Toroidal plasma confinement devices having a rotational transform of the magnetic field (such as stellarators) are sensitive to small coil misalignments, which cause global distortions of the magnetic field. Such low-order, long-scale-length perturbations can have Fourier components that resonate with rational values of transform and break closed flux surfaces, leading to the loss of plasma.[1-3] In stellarator-type systems, the rotational transform is produced by coils external to the plasma, and the magnitudes of error field components that resonate geometrically with the rotational transform must be restricted to $\sim 10^{-3} B_o$ (where B_o is the toroidal field) by maintaining coil alignment tolerances.

One member of the stellarator family is the torsatron.[4-6] It is particularly attractive as an experimental device because highly sheared fields can be obtained and the absence of toroidal field (TF) coils offers good access to the plasma. However, conventional torsatrons require a substantial vertical field from outboard coils to cancel the the net vertical field of the unidirectional helical windings. If the vertical field (VF) coils are not concentric with the major axis of the helical coils, a long-scale-length error field is produced. Numerical studies using the ORNL Advanced Toroidal Facility (ATF) torsatron configuration (major radius R_o = 2.1 m) have shown that the VF coils must be centered to within 1 cm if closed flux surfaces are to be maintained.

An earlier study[7] showed in principle how the axes of the VF and helical coil sets of the ATF torsatron (an l = 2 device) can be determined by separately exciting coil pairs and mapping the resulting

magnetic field. This work outlined methods by which coil alignment can be measured and optimized by measuring components of $\vec{B}$ along and near the major axis of the torus. The strategy is to use field nulls to determine the location of the net dipole moment of each coil pair. When all of these moments are aligned, the performance is optimized.

This method has numerous advantages: (1) it does not require a vacuum, (2) it can be carried out in steady state at reduced fields, (3) it indicates the cause of the field error and the direction of coil movement for correction, (4) it can be performed during the assembly of the device, (5) it requires measurements only near the symmetry axis (R = 0), that is, well away from the confinement volume, and (6) it aligns the coil magnetic (rather than mechanical) axes.

In this paper, we apply these ideas to the actual experimental determination of the alignment of the axes of the helical and VF coil sets of the l = 3 URAGAN-3 device. Electron beam mapping[8] of fields in the URAGAN-3 device has indicated that the region of plasma confinement is smaller than calculated, presumably because of a field error such as that produced by coil misalignments. Magnetic field and flux surface calculations were made using the geometry of the URAGAN-3 torsatron, and experiments were then undertaken to determine whether there were coil misalignments that could explain the observed plasma size.

Section II describes the URAGAN-3 device and the behavior of its flux surfaces and also shows calculated flux surfaces that would result from small misalignment errors. Experiments to determine whether errors were present and to separately find the major axes of the VF and helical coil sets are detailed in Sec. III. Results and conclusions are presented in Sec. IV.

II. CALCULATED FLUX SURFACES IN URAGAN-3

URAGAN-3 is an l = 3 torsatron[9] with the coil configuration shown in Fig. 1. It has a major radius of R_0 = 1.0 m, a minor radius of 26 cm, and a winding law $\phi = -3/9(\theta - 0.2 \sin \theta - 0.1 \sin 2\theta)$, where θ and ϕ are the poloidal and toroidal angles, respectively. All coils are powered in series from a flywheel generator, with shunts provided to

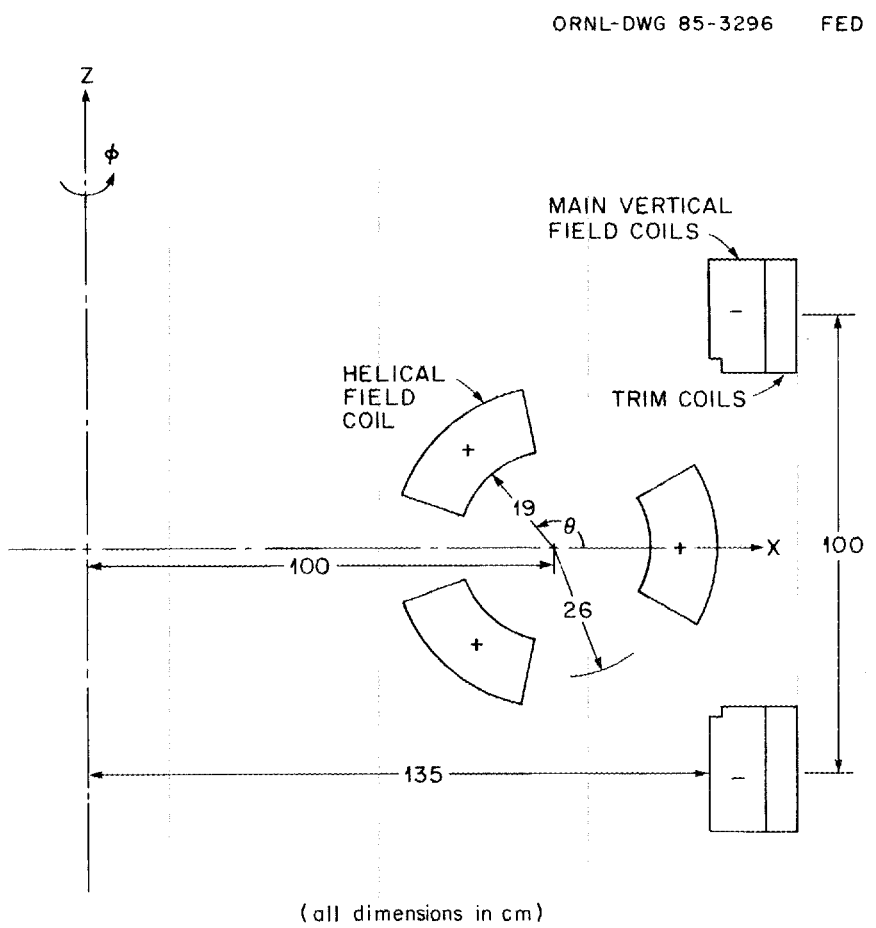

Fig. 1. Cross-sectional view of the URAGAN-3 coil system. Pluses and minuses indicate current flow direction under normal operation. Dimensions are in centimeters.

vary the relative currents in the VF and trim coils. Typically, a toroidal field of 1 T is generated at the magnetic axis of the plasma.

Figure 2 shows the current filament model used to model the conductors in URAGAN-3. For flux surface calculations, each of the helical coils is modeled with 20 filaments, and each of the VF coils

ORNL-DWG 85-3406 FED

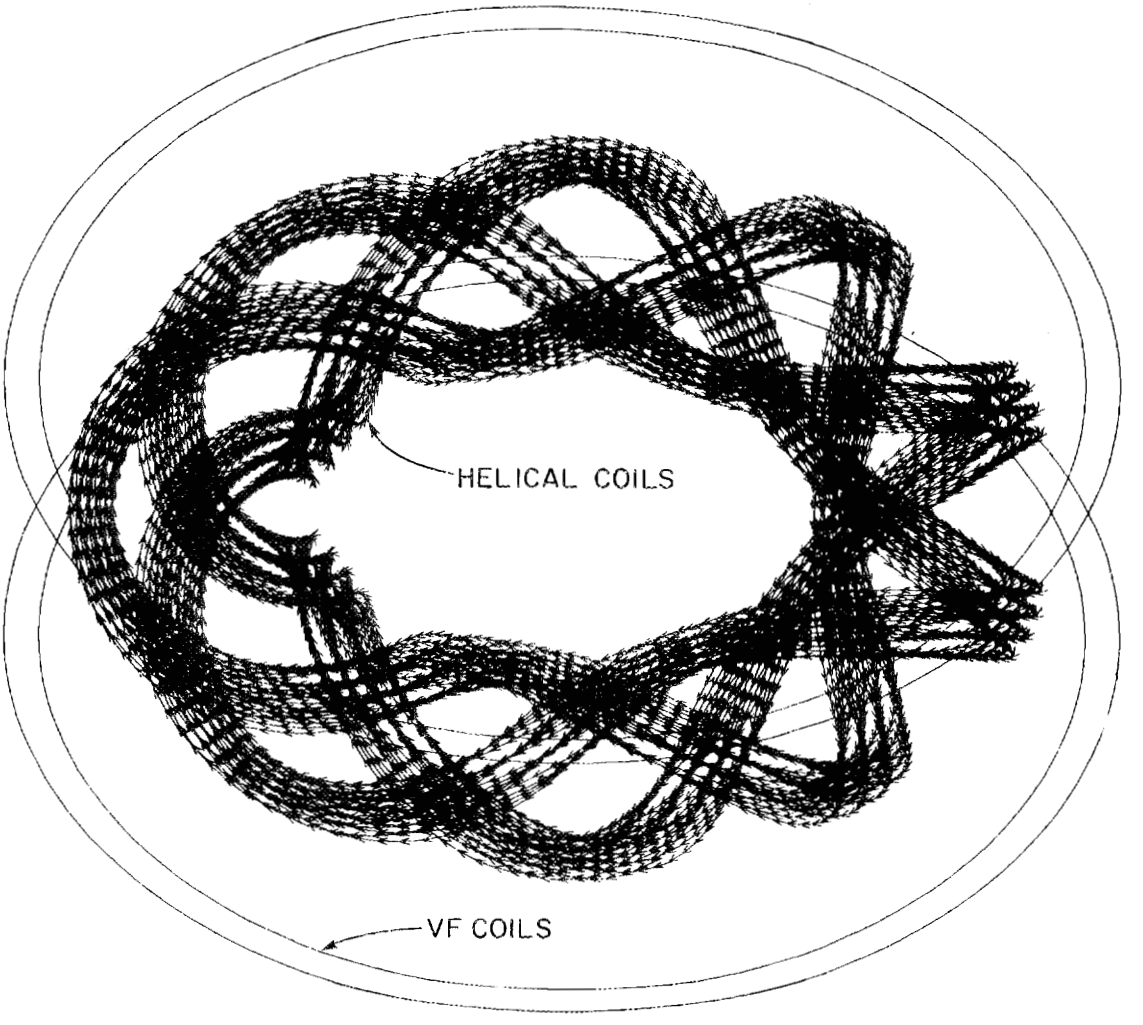

Fig. 2. Three-dimensional view of the current filament model used in calculating flux surfaces in URAGAN-3.

(which are far from the plasma) is represented by a single filament. For the calculations of the magnetic field maps (of the region near R = 0) used in alignment measurements, all the coils could be adequately represented by single filaments.

Figure 3a shows closed flux surfaces with ideal coil alignment in URAGAN-3. The flux surfaces are calculated by following field lines

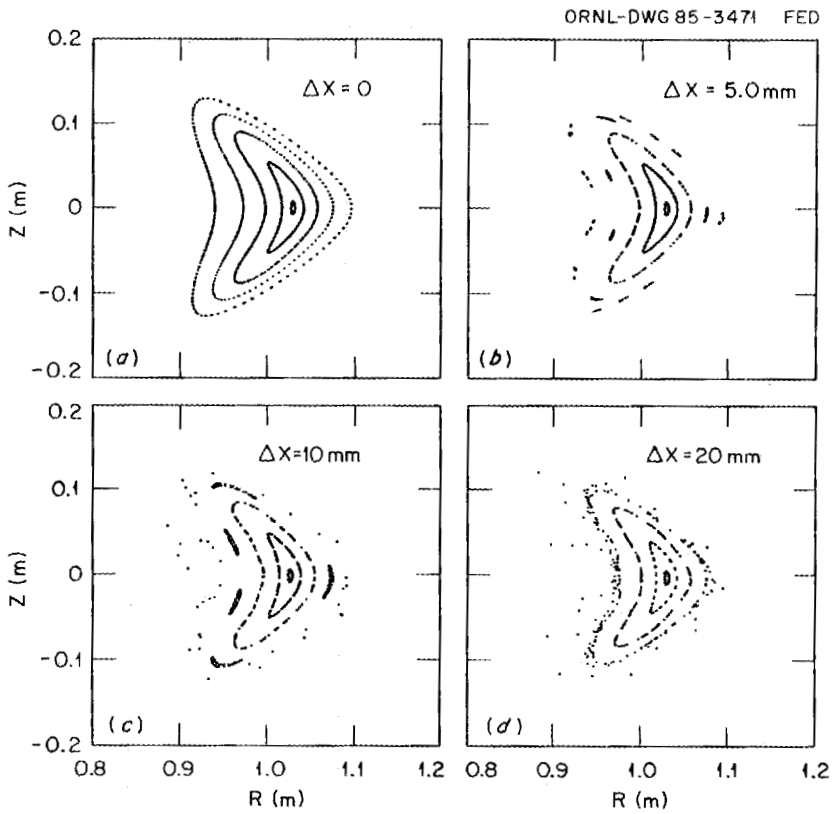

Fig. 3. Flux surfaces in URAGAN-3, showing (a) all coils correctly aligned, (b) VF coil displacement ΔX = 0.5 cm, (c) ΔX = 1.0 cm, and (d) ΔX = 2.0 cm. The current in each of the three helical coils was 555 kA, and a total of 461 kA flowed through the VF and trim coils. This helical field current gives an axial field of 1 T.

for at least 100 toroidal transits or until they leave the plasma volume. One point was plotted per transit. For the configuration shown here, the rotational transform rises from $\iota_0 \approx 0.02$ at the magnetic axis to $\iota_a \approx 0.30$ at the plasma edge.

One of the most likely alignment errors is a horizontal displacement of the VF coils with respect to the helical coils. A shift of the VF coils by 0.5 cm (see Fig. 1) results in a global, long-wavelength field error that breaks up the outermost flux surface. This is shown in Fig. 3b. Larger horizontal shifts cause even more breakup of the flux surfaces, as shown in Figs. 3c and 3d. For $\Delta X \gtrsim 1$ cm, the average minor radius of the last flux surface is reduced by a factor of ~2. Other types of alignment errors, such as coil tilts or the horizontal displacement of a single coil, are, of course, also possible, but these errors were not found in URAGAN-3.

III. MAGNETIC FIELD MEASUREMENTS

A. Procedure

A large number of magnetic field calculations were carried out prior to the actual field measurements in order to map the various magnetic field components near R = 0 with and without coil alignment errors present for various configurations of coil currents. The general experimental strategy suggested by this work was as follows:

1. Determine the spatial structure of the magnetic field near R = 0 with both the VF and helical coils energized; this measurement quickly shows whether errors are present, but does not give precise axis locations.
2. Determine the magnetic symmetry axis of the helical coils.
3. Determine the magnetic symmetry axis of the VF coils.

4. Realign the coils and check the relative locations of the coil axes.

If alignment errors were revealed in the first step, then details of these deviations would be ascertained in steps 2 and 3, and step 4 could be taken to realign the coils.

Only a few of the many field plots originally generated were directly used in the experiments. Those plots are shown along with details of the measurements in the following sections.

B. Apparatus

Magnetic fields were measured by means of sensors placed on a positioning probe. A schematic view of this probe is shown in Fig. 4. The magnetic field sensor was attached to a stiff wire that could be moved through 3 m in the vertical direction. The sensor position could be varied by 0.2 m in radius, via a screw drive, and by 360° in toroidal azimuth (ϕ). Magnetic field sensor positions were measured by means of potentiometers driven by gears, and the potentiometer readings were recorded by a computer. The analog-to-digital converter of the computer limited the positional accuracy of the probe to 1.5 mm in the Z direction, 0.1 mm in radius, and 0.1° in the angle ϕ.

Two types of magnetic field sensors were used: a magnetodiode[10] and a Hall effect probe. The magnetodiode was sensitive to fields of ~30 mG, and the Hall effect probe could detect fields as low as 10 mG. These probes could be mounted so as to detect B_R, B_ϕ, or B_Z; the field readings were relayed to a computer. The magnetic field coils in URAGAN-3 were operated steady state, but with currents reduced by a factor of 10 to 20 relative to the normal operating values to prevent

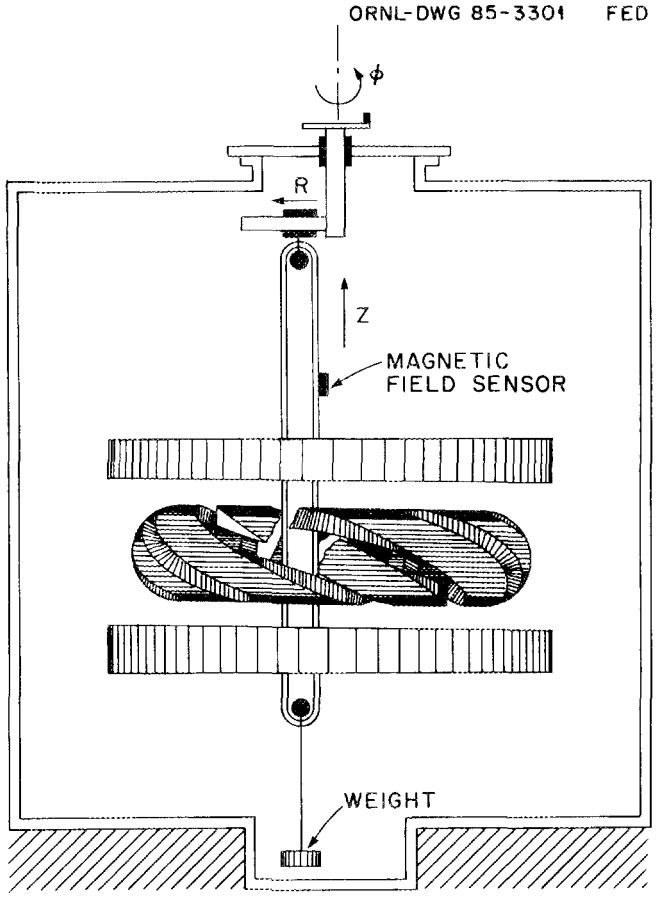

Fig. 4. Schematic view of the probe positioning device inside URAGAN-3.

coil overheating. The ability to run continuously greatly facilitated the measurements.

C. Overall Magnetic Field System Tests

In order to determine if alignment errors were present, the coils were energized in their normal configuration (Fig. 5a). However, the ratio of the helical to VF coil currents was increased above its usual

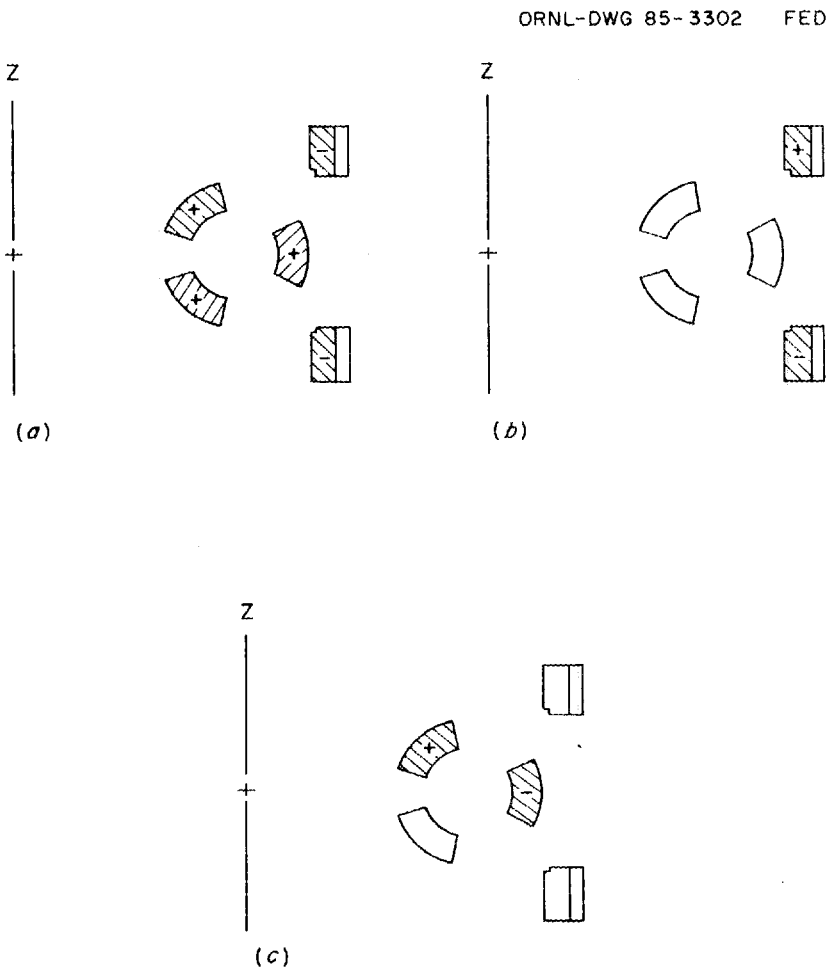

Fig. 5. Cross-sectional views of the coil system in URAGAN-3, showing current flow directions: (a) normal current configuration, (b) currents applied during measurement of the VF coil set axis, and (c) currents applied during measurement of the helical coil set axis.

value. Under these conditions, and with the coil sets correctly aligned, calculations show that there is a point on the Z axis where B_Z changes sign. This change is quite sharp, as shown in Fig. 6, which plots B_Z contours in three X-Y planes spaced at 1-cm intervals along the Z axis.

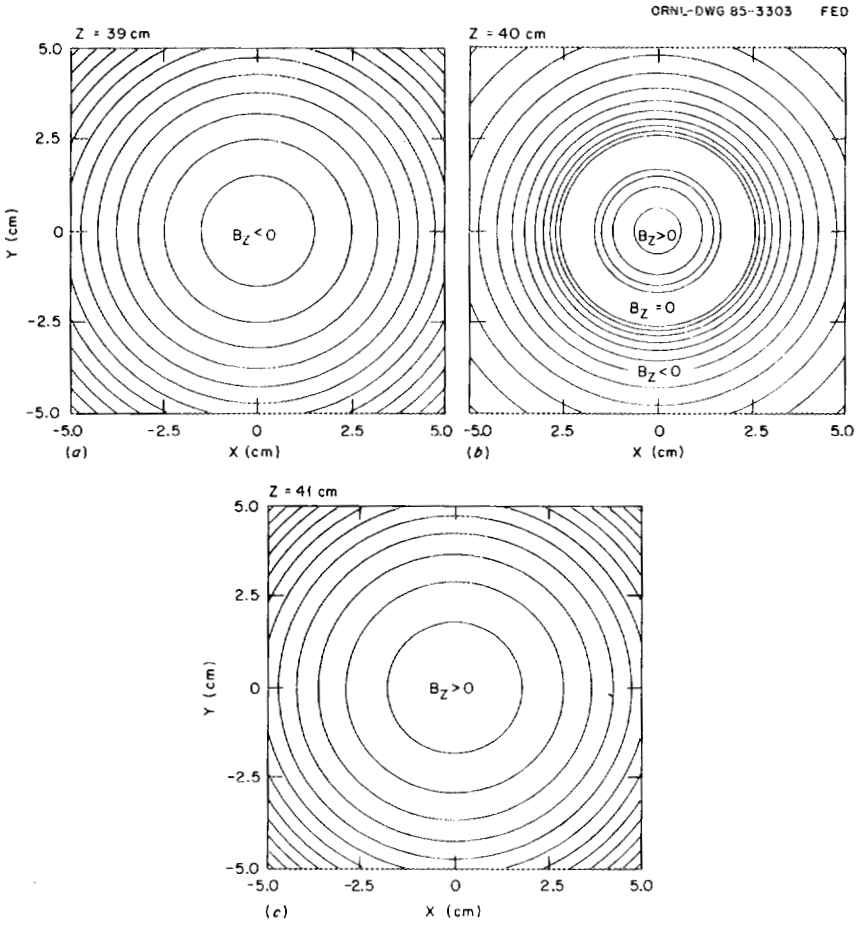

Fig. 6. B_Z values in three X-Y planes spaced 1 cm apart in Z, with correct coil alignment. The relative coil currents were chosen to produce a null in B_Z at Z = 40 cm.

If the VF coils are shifted 1 cm in the X direction with respect to the helical coils, these plots are significantly changed. The center of the B_Z contours undergoes a large shift in the X direction, alternating from plus to minus as B_Z goes through zero, as is shown in Fig. 7.

In the calculations shown in Figs. 6 and 7, the relative VF and helical coil currents were chosen to produce a null in B_Z in the

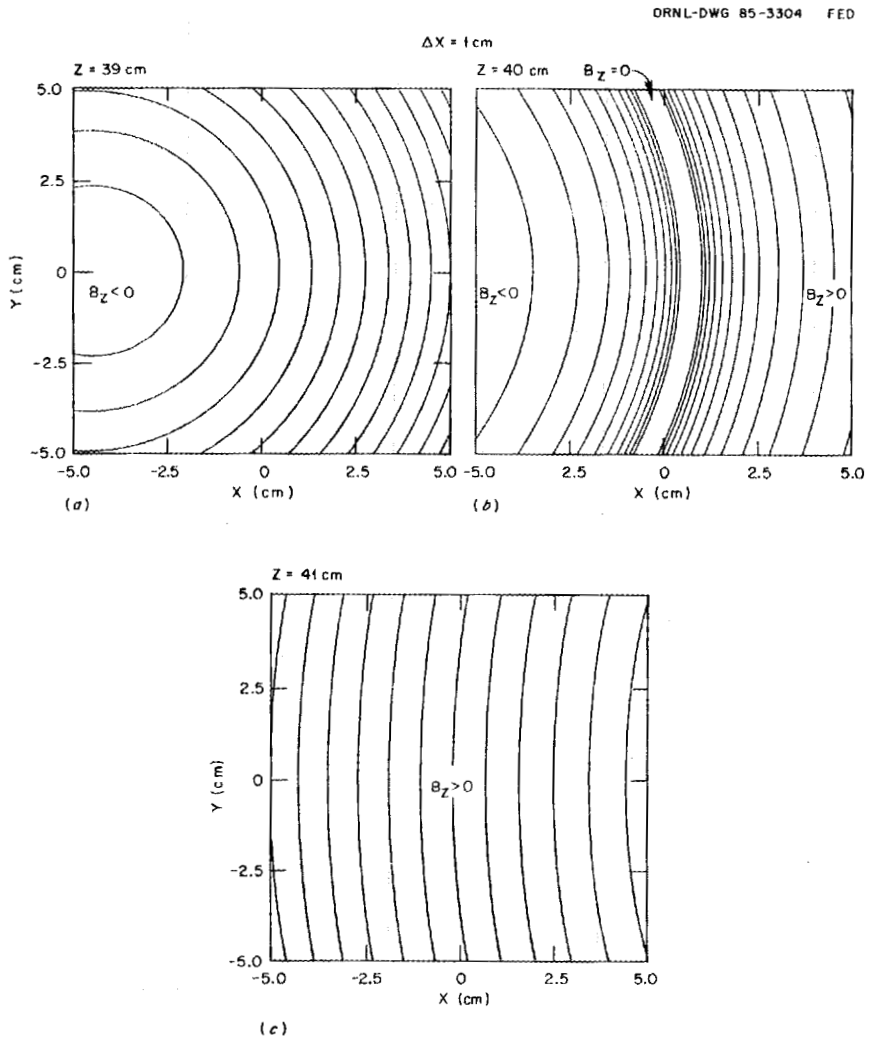

Fig. 7. B_Z contours in the three planes shown in Fig. 8, but with the VF coils shifted by ΔX = 1.0 cm.

Z = 40-cm plane. Since it is the spatial structure of the field (rather than its absolute magnitude) that is critical, the currents used in the actual experiment can be chosen to place the B_Z = 0 region at an experimentally convenient value of Z; the field patterns will show qualitatively the same structure.

To test for the suspected type of alignment error (i.e., a shift of the axis of the VF coils) in URAGAN-3, B_Z was measured in each of several X-Y planes along Z by keeping the magnetic field sensor fixed in radius and rotating the probe in angle. The results are shown in Fig. 8 and exhibit regular oscillations in B_Z as ϕ is scanned in a circle. Note that at Z = 113.5 cm, B_Z twice passes through zero, as would be expected from Fig. 7b, and that for smaller values of Z, B_Z is negative. Scans were made continuously in ϕ. The small difference in the B_Z values at $\phi = 0°$ and $\phi = 360°$ is due to drift in the generator currents during the scan; this error does not change the conclusions of the measurements.

The waveforms in Fig. 8 are consistent with those expected for the field plots in Fig. 7, which were calculated for a coil shift of ΔX = 1 cm. The sinusoidal behavior observed is contrary to that expected for perfect alignment (see Fig. 6), which would result in constant (straightline) values of $B_Z(\phi)$ at constant R and Z. From these measurements it could be concluded that there was indeed an error in the alignment of the URAGAN-3 helical and VF coil sets.

D. Separate Determination of the VF and Helical Coil Axes

1. Axis of the VF Coils

Once it was known that an alignment error existed, the next step was to separately measure the Z axis of each coil set in order to determine the size and direction of the misalignment. The axis of the VF coils was determined by exciting the top and bottom VF coils with opposing currents, as is indicated in Fig. 5b. This axis was measured at several points along the Z axis, as listed in Table I. The contours

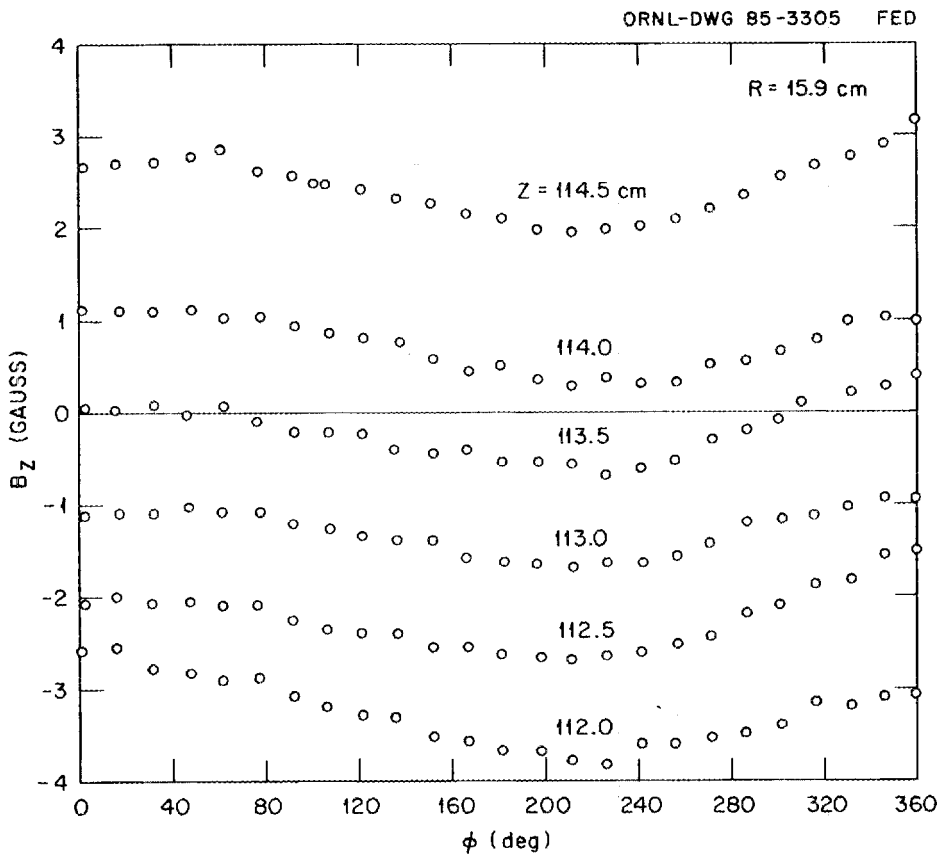

Fig. 8. Measured B_Z values as a function of angular probe rotation about the Z axis for six different positions in Z. The relative coil currents were chosen to produce a null in B_Z in the Z = 113.5-cm plane. The probe was located at a radius of 15.9 cm relative to the assumed center of the coil sets.

of B_R are found to be symmetric, as shown in Fig. 9 for the X-Y plane at Z = 0.

The measurements were made by scanning in radius about preselected values of B_R for each of six azimuthal positions (see Fig. 9a). Several data points were taken for each radial scan, and a linear

Table I. Measurements of coil axis locations

FIELD	Z (cm)	X (cm)	Y (cm)	ERROR (cm)
VF	130	1.52	1.10	0.09
VF	110	1.43	0.63	0.08
VF	90	0.92	0.41	0.17
VF	60	1.36	0.45	0.08
VF	50	1.43	0.31	0.07
VF	10	1.34	0.31	0.08
VF	10	1.32	-0.12	0.16
VF	-30	1.23	0.01	0.09
VF	-50	1.18	0.31	0.11
VF	-70	2.18	-0.44	0.55
Helical	50	0.34	-0.05	0.05
Helical	40	0.43	0.06	0.09
Helical	30	0.40	-0.13	0.10
Helical	10	0.34	0.11	0.03
Helical	0	0.42	-0.12	0.05
Helical	0	0.24	-0.15	0.07
Helical	0	0.39	0.03	0.07
Helical	-10	0.38	-0.24	0.10
Helical	-30	0.36	-0.24	0.04
Helical	-40	0.31	0.03	0.05
VF	55	0.20	0.16	0.11
VF	45	0.36	0.20	0.10
VF	25	0.50	0.13	0.05
VF	5	0.50	0.13	0.08
VF	-25	0.46	0.03	0.03
VF	-35	0.37	0.08	0.10
VF	-55	0.37	0.08	0.19

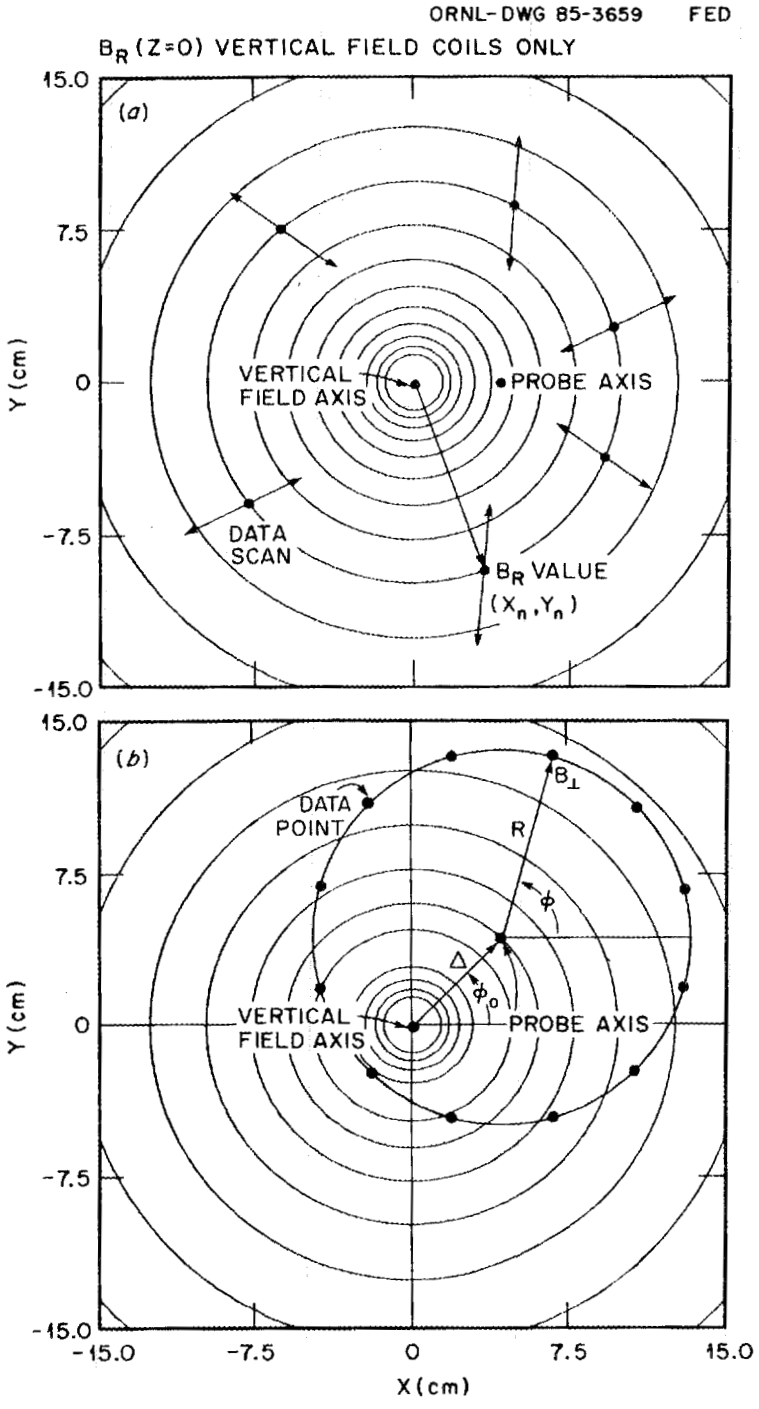

Fig. 9. B_R contours in the Z = 0 plane for the case in which the VF coils were powered with opposite currents. (a) Data scan ranges for the initial VF axis determination measurements. (b) Geometry and data points for the final VF axis determination after the VF coils were shifted.

regression analysis was performed to interpolate to the same B_R values for each radial scan. The six B_R values so determined were then used to find the axis of the B_R field relative to the probe axis via a minimization technique. The X and Y values found by this method are given in Table I, along with the error, which is defined from the minimization technique as

$$\text{VF error} = \sum_{n=1}^{6} \frac{|R - (X_n^2 + Y_n^2)^{1/2}|}{6} ,$$

where R is the radius from the measured center and X_n and Y_n are the coordinates of each data point (as indicated in Fig. 9a). Note that the largest error is 0.17 cm, which indicates that the measured points were close to a circle of radius R. However, there is some scatter in the values of X and Y listed in Table I. This scatter arises from system errors such as pickup of the large B_Z fields that are present, drifts in the coil current during a B_R scan, small oscillations of the probe positioning apparatus, and the horizontal component of the earth's magnetic field. This last effect was ~0.2 G, which is sufficient to cause a shift of the apparent coil axis $\Delta X \sim 0.2$ cm toward the reference axis. Improvements to the measurement technique during the coil alignment process ultimately greatly reduced these system errors, as described in Sec. II.D.3.

2. Axis of the Helical Coils

To locate the axis of the helical coils, two coils were excited with oppositely directed currents, as shown in Fig. 5c. Two different helical coil pairs were powered during the course of the experiments to check for systematic errors. In the same manner as before, data were

taken in X-Y planes at several points along the Z axis, as listed in Table I.

When only helical coils are powered, the contours of B_R are decidedly nonaxisymmetric but periodic in ϕ, as is illustrated in Fig. 10. Since the coils are helical, B_R oscillates from positive to negative, passing through zero at six points. Data points were taken in the region of these six null points, and a linear regression analysis was performed to find the nulls. A computer program was written to find (by interpolation) the point of crossing of the three

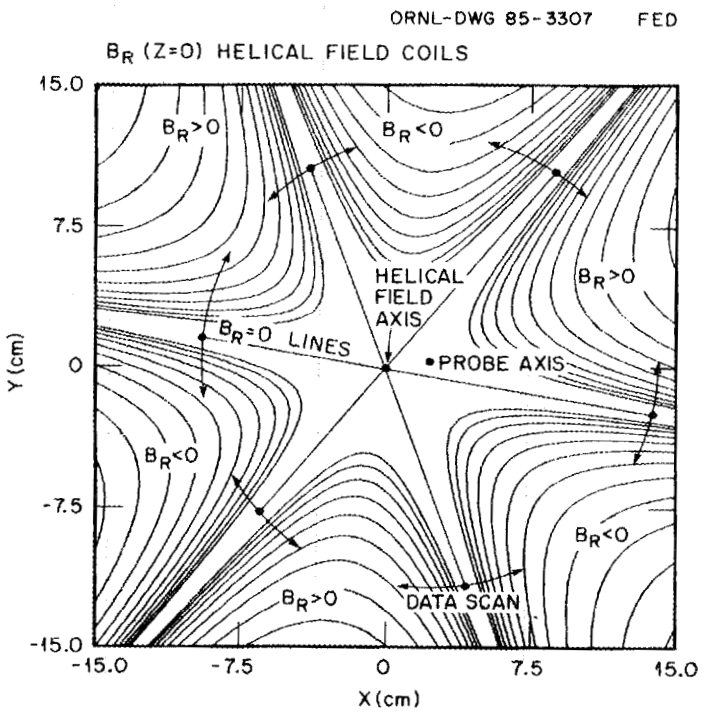

Fig. 10. B_R contours in the Z = 0 plane for the case in which two helical coils were powered. Azimuthal data scan ranges are indicated, together with lines connecting measured B_R = 0 points. These lines intersect at the helical field axis.

lines connecting the null points. Because of experimental errors, the three lines did not quite cross at a single point but formed a triangle. The perpendicular distance from the center of the triangle (which was taken as the measured helical field axis) to each of the sides was d_n, and the experimental error was defined (again, from the minimization technique used) as

$$\text{helical error} = \sum_{n=1}^{3} \frac{|d_n|}{3} \quad .$$

Values of this error are given in Table I and are quite small. The same systematic errors that affected the VF measurements were also present in these measurements. However, sensitivity studies of the effect of the earth's field showed that, in this case, it has a negligible effect on the calculated coil centers. This explains why this case exhibits less spread in the measured X and Y values (given in Table I) than was present for the VF coils.

The measured vertical and helical axis points, as projected onto a single plane, are plotted in Fig. 11. Despite the scatter in the initial vertical field axis points, it is clear that there existed a systematic shift of about a centimeter between the axes of the two coil systems, necessitating realignment.

3. Axis of the VF Coils After Realignment

The simplest way to improve the relative alignment of the coil sets was to move the less complicated and lighter VF coils. After the VF coils were adjusted in the direction indicated in Fig. 11, measurements were made to check their alignment with the helical coils.

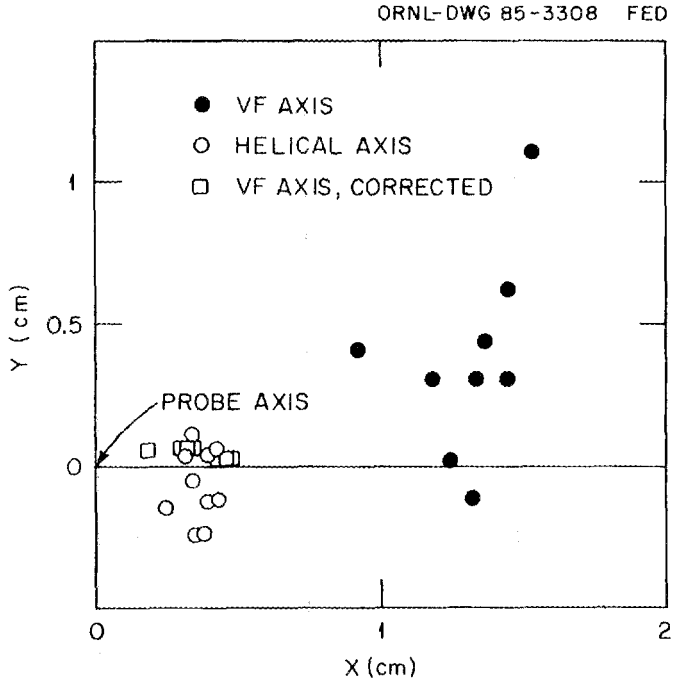

Fig. 11. Measured values for the helical coil and VF coil axes plotted in a single X-Y plane.

Improvements in the original method of taking data were implemented during these later measurements. The earth's magnetic field was subtracted by taking data in a preliminary scan with all coils turned off. With the coils powered in the configuration shown in Fig. 5b (vertical field axis determination), small variations in coil currents during a measurement scan were compensated by dividing the measured field by the instantaneous coil current, and errors due to pickup of the large B_Z field were compensated.

The geometry of these measurements is shown in Fig. 9b. If the probe axis is located a distance Δ and angle ϕ_o from the magnetic dipole axis of the VF coils, then

$$B_\perp = \alpha R \left[1 - \frac{\Delta}{R} \cos(\phi - \phi_o)\right] + B_o \ ,$$

where $B_\perp$ is the radial field measured by the probe and the B_o term results from the fraction of the large B_Z field that is present and is picked up by the probe due to imperfect alignment. The constant α was determined by measuring $B_\perp$ at two values along a probe radius and using the relation $\alpha = (B_{\perp 1} - B_{\perp 2})/(R_1 - R_2)$. Then the probe was rotated in ϕ, data were taken at 30° intervals, and the maximum and minimum values of $B_\perp$ were found. B_o was calculated from the rotation data using $B_o = (1/2)(B_{\perp max} - B_{\perp min}) - \alpha R$. Once α and B_o were determined, the original $B_\perp$ equation was solved for Δ and ϕ_o by a minimization technique. Coordinates of the resulting axis locations are listed in Table I.

The errors listed in the table for these measurements were found from the minimization technique to be

$$\text{VF error} = R \left[\frac{1}{12} \sum_{n=1}^{12} \frac{(B_{\perp calc} - B_{\perp meas})^2}{\bar{B}^2_{\perp meas}} \right]^{1/2} ,$$

where $B_{\perp calc}$ and $B_{\perp meas}$ are the calculated and measured values of $B_\perp$, respectively, determined at 30° intervals in ϕ, and $\bar{B}_{\perp meas}$ is the mean of the measured $B_\perp$ values. There is considerably less scatter in these data points than in the earlier measurements because systematic errors due to the earth's field, drift in the coil currents, and unwanted components of B_Z have been eliminated.

Coordinates for the magnetic dipole axis of the VF coils after realignment are plotted in Fig. 11. These points are very close to those of the helical coils, indicating that the two coil systems are now aligned.

The improved magnetic measurements also showed no trend in axis location for planes at different Z values, which made it possible to eliminate VF axis tilts and misalignments of a single VF coil from consideration. These findings were supported by careful mechanical measurements.

IV. DISCUSSION OF RESULTS

Before the VF and helical coil sets were aligned, the flux surfaces of URAGAN-3 were mapped experimentally using low-energy electrons.[4] Results of this flux surface mapping are shown in Fig. 12. Note that the closed flux surface area is similar to the one calculated

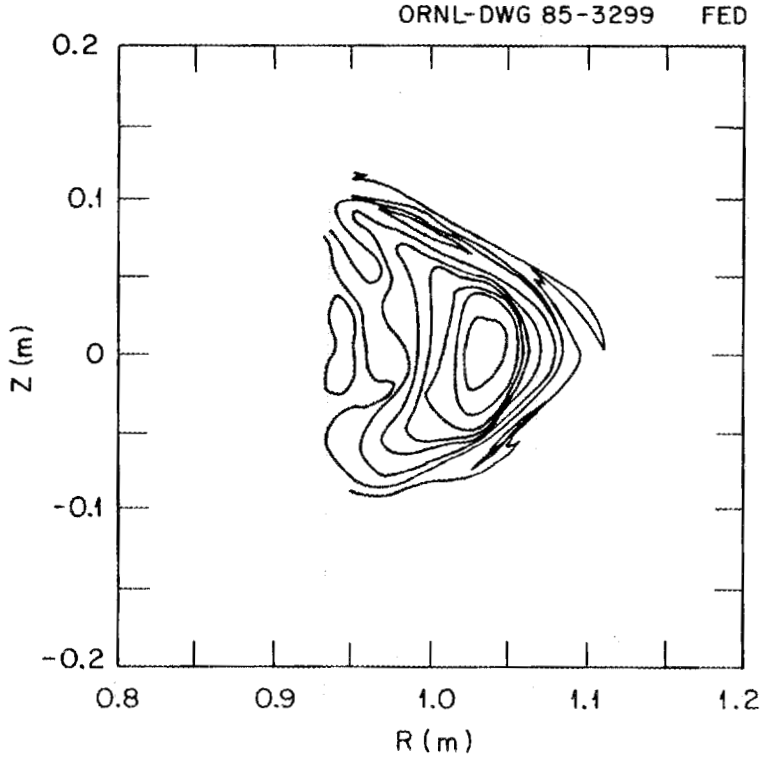

Fig. 12. Experimentally mapped flux surfaces in URAGAN-3 (from Ref. 8).

in Fig. 3c and that the breakup of the outer flux surfaces suggests that field errors were present.

Analysis of the number of electron beam transits around the torus is shown in Fig. 13. This analysis shows a core region (enclosed by contours 1 and 2 in Fig. 13a) in which more than ten beam transits were recorded. Outside this region lies a zone ~5 cm wide in which stochastic behavior of the flux surfaces is observed, again suggesting the possibility of alignment errors. However, these measurements must be intepreted with care because these data were taken with a 9% imbalance in the currents in the two VF coils, which was empirically chosen to optimize the flux surfaces. This suggests the possible presence of an additional radial error field due to misalignments within the helical coil set itself. Such an error would be compensated by the VF coil current imbalance and would not be detected with the alignment technique described here.

The methods developed during these experiments are generally applicable to coil alignment in other torsatrons, although details may vary depending on the exact coil geometry. This method has the advantage of determining the magnetic dipole (rather than the mechanical) axes of the coils directly. It is necessary to know only the order of magnitude of the coil currents, since the measurements depend only on the geometry of the coils. Since it is not necessary to make field measurements at precisely R = 0 or in the region of the plasma, the magnetic field sensor can be mounted from a rigid post at the estimated center of the coil sets. The measurements do not require that the system be under vacuum, and either steady-state or pulsed currents can be employed.

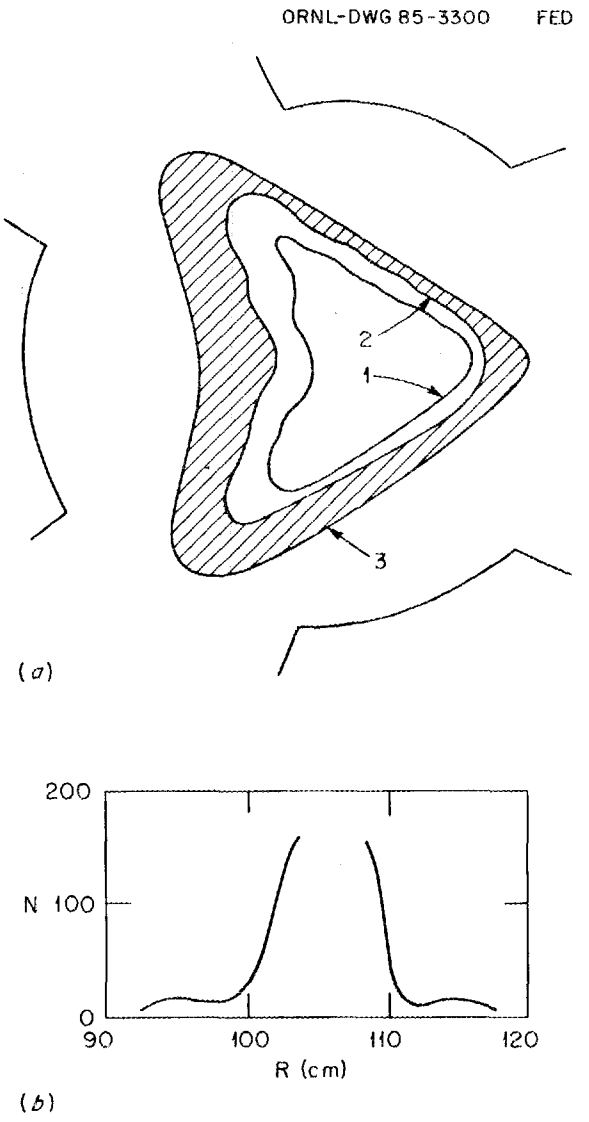

Fig. 13. Electron beam map of flux surfaces in URAGAN-3 and the number of electron beam transits of the device. (a) Flux surfaces. Inside the hatched area (between contours 2 and 3) the beam exhibited ergodic behavior. Between contours 1 and 2, 10 to 20 electron beam transits were observed. More than 30 traversals were measured inside contour 1. (b) The number of beam transits as a function of major radius.

It should be noted that the alignment technique described here is primarily useful for aligning the coil axes. Since the field measurements are made in the vicinity of the symmetry axis ($R = 0$), they are relatively insensitive to distortions such as ellipticity of the VF coils. Errors such as these would be better diagnosed using a technique that involved field measurements nearer the coils, where the effect of small distortions is much stronger.

ACKNOWLEDGMENTS

This work was carried out as part of a U.S.-U.S.S.R. exchange in fusion research. We are grateful to V. S. Taran, A. A. Utkin, G. P. Opaleva, and M. I. Zolototrubova for their technical assistance with the experiments. We would also like to thank V. T. Tolok, Yu. K. Kuznetsov, J. F. Lyon, J. L. Dunlap, J. L. Shohet, and R. A. Blanken for their support and encouragement. The work of the U.S. scientists was supported by the Office of Fusion Energy, U.S. Department of Energy, under Contract No. DE-AC05-84OR21400 with Martin Marietta Energy Systems, Inc., and Contract No. DE-AC02-02-84-ER53166 with the University of Wisconsin.

REFERENCES

1. M. S. Berezhetskij, S. E. Grebenshchikov, I. A. Kossyi, Yu. I. Nechaev, M. S. Rabinovich, I. S. Sbitnikova, and I. S. Shpigel, in Plasma Physics and Controlled Nuclear Fusion Research (International Atomic Energy Agency, Vienna, 1969), Vol. 1, p. 529 (in Russian).
2. A. I. Morozov and L. S. Solov'ev, in Reviews of Plasma Physics (Consultants Bureau, New York, 1966), Vol. 2.
3. L. S. Solov'ev and V. D. Shafranov, in Reviews of Plasma Physics (Consultants Bureau, New York, 1970), Vol. 5.
4. C. Gourdon, D. Marty, E. K. Maschke, and J. P. Dumot, in Plasma Physics and Controlled Nuclear Fusion Research (International Atomic Energy Agency, Vienna, 1969), Vol. I, p. 847.
5. I. S. Danilkin and I. S. Shpigel, Tr. Fiz. Inst. Akad. Nauk SSSR 65, 50 (1976) (in Russian).
6. B. A. Carreras, H. R. Hicks, J. A. Holmes, V. E. Lynch, L. Garcia, J. H. Harris, T. C. Hender, and B. F. Masden, Phys. Fluids 26, 3569 (1983).
7. J. A. Rome, J. H. Harris, G. H. Neilson, and T. C. Jernigan, A Novel Method of Aligning ATF-1 Coils, Oak Ridge National Laboratory Report No. ORNL/TM-8496, 1983.
8. A. V. Georgievskij, Yu. V. Gutarev, A. G. Dikij, et al., in Proceedings of the 12th European Conference on Plasma Physics and Controlled Nuclear Fusion Research, Budapest (1985).

9. A. V. Bazaeva, V. E. Bykov, A. K. Georgievskij, and V. G. Peletminskaya, Proceedings of the Second All-Union Conference on Fusion Reactor Technology, Leningrad (1981) Vol. 1, pp. 31-38 (in Russian).

10. V. I. Stafeev and Eh. I. Karakashan, Magnetodiodes (Nauka Press, Moscow, 1975) (in Russian).

ORNL/TM-9685

Dist. Category UC-20

INTERNAL DISTRIBUTION

1. L. A. Berry
2. B. A. Carreras
3-7. R. J. Colchin
8. R. A. Dory
9. J. L. Dunlap
10. P. H. Edmonds
11. J. C. Glowienka
12-16. J. H. Harris
17. G. R. Haste
18. C. L. Hedrick
19. D. L. Hillis
20. S. Hiroe
21. T. C. Jernigan
22. D. V. Jett
23. R. L. Johnson
24-25. D. K. Lee
26. J. F. Lyon
27. M. Murakami
28. G. H. Neilson
29. B. E. Nelson
30. D. A. Rasmussen
31. R. K. Richards
32-33. J. A. Rome
34. P. B. Thompson
35. N. A. Uckan
36. T. Uckan
37. J. B. Wilgen
38. J. Sheffield
39-40. Laboratory Records Department
41. Laboratory Records, ORNL-RC
42. Document Reference Section
43. Central Research Library
44. Fusion Energy Division Library
45-46. Fusion Energy Division Publications Office
47. ORNL Patent Office

EXTERNAL DISTRIBUTION

Kharkov Physico-Technical Institute, Ukrainian Academy of Sciences, Kharkov 310108, U.S.S.R.

48-49. S. I. Fedotov

50-51. F. I. Ozherel'ev

52-53. O. S. Pavlichenko

54-55. D. P. Pogozhev

56-57. V. M. Zalkind

58-59. J. Treffert, Torsatron/Stellarator Laboratory, University of Wisconsin, Madison, WI 53706

60. Office of the Assistant Manager for Energy Research and Development, Department of Energy, Oak Ridge Operations Office, P. O. Box E, Oak Ridge, TN 37831

61. J. D. Callen, Department of Nuclear Engineering, University of Wisconsin, Madison, WI 53706

62. J. F. Clarke, Office of Fusion Energy, Office of Energy Research, ER-50, Germantown, U.S. Department of Energy, Washington, DC 20545

63. R. W. Conn, Department of Chemical, Nuclear, and Thermal Engineering, University of California, Los Angeles, CA 90024

64. S. O. Dean, Director, Fusion Energy Development, Science Applications International Corporation, Gaithersburg, MD 20879

65. H. K. Forsen, Bechtel Group, Inc., Research Engineering, P. O. Box 3965, San Francisco, CA 94105

66. J. R. Gilleland, GA Technologies, Inc., Fusion and Advanced Technology, P.O. Box 81608, San Diego, CA 92138
67. R. W. Gould, Department of Applied Physics, California Institute of Technology, Pasadena, CA 91125
68. R. A. Gross, Plasma Research Library, Columbia University, New York, NY 10027
69. D. M. Meade, Princeton Plasma Physics Laboratory, P.O. Box 451, Princeton, NJ 08544
70. M. Roberts, International Programs, Office of Fusion Energy, Office of Energy Research, ER-52, U.S. Department of Energy, Washington, DC 20545
71. W. M. Stacey, School of Nuclear Engineering and Health Physics, Georgia Institute of Technology, Atlanta, GA 30332
72. D. Steiner, Nuclear Engineering Department, NES Building, Tibbetts Avenue, Rensselaer Polytechnic Institute, Troy, NY 12181
73. R. Varma, Physical Research Laboratory, Navrangpura, Ahmedabad 380009, India
74. Bibliothek, Max-Planck Institut fur Plasmaphysik, D-8046 Garching, Federal Republic of Germany
75. Bibliothek, Institut fur Plasmaphysik, KFA, Postfach 1913, D-5170 Julich, Federal Republic of Germany
76. Bibliotheque, Centre des Recherches en Physique des Plasmas, 21 Avenue des Bains, 1007 Lausanne, Switzerland
77. Bibliotheque, Service du Confinement des Plasmas, CEA, B.P. No. 6, 92 Fontenay-aux-Roses (Seine), France

78. Documentation S.I.G.N., Departement de la Physique du Plasma et de la Fusion Controlee, Centre d'Etudes Nucleaires, B.P. 85, Centre du Tri, 38041 Grenoble, France
79. Library, Culham Laboratory, UKAEA, Abingdon, Oxfordshire, OX14 3DB, England
80. Library, FOM-Instituut voor Plasma-Fysica, Rijnhuizen, Edisonbaan 14, 3439 MN Nieuwegein, The Netherlands
81. Library, Institute of Plasma Physics, Nagoya University, Nagoya 464, Japan
82. Library, International Centre for Theoretical Physics, Trieste, Italy
83. Library, Laboratorio Gas Ionizatti, CP 56, I-00044 Frascati, Rome, Italy
84. Library, Plasma Physics Laboratory, Kyoto University, Gokasho, Uji, Kyoto, Japan
85. Plasma Research Laboratory, Australian National University, P.O. Box 4, Canberra, A.C.T. 2000, Australia
86. Thermonuclear Library, Japan Atomic Energy Research Institute, Tokai-mura, Ibaraki Prefecture, Japan
87. G. A. Eliseev, I. V. Kurchatov Institute of Atomic Energy, P. O. Box 3402, 123182 Moscow, U.S.S.R.
88. V. A. Glukhikh, Scientific-Research Institute of Electro-Physical Apparatus, 188631 Leningrad, U.S.S.R.
89. I. Shpigel, Institute of General Physics, U.S.S.R. Academy of Sciences, Ulitsa Vavilova 38, 177924 Moscow, U.S.S.R.

90. D. D. Ryutov, Institute of Nuclear Physics, Siberian Branch of the Academy of Sciences of the U.S.S.R., Sovetskaya St. 5, 630090 Novosibirsk, U.S.S.R.

91. V. T. Tolok, Kharkov Physical-Technical Institute, Academical St. 1, 310108 Kharkov, U.S.S.R.

92. Jin Shang-Xian, Graduate School, Academia Sinica, P.O. Box 3908, Beijing, China (PRC)

93. R. A. Blanken, Experimental Plasma Research Branch, Division of Applied Plasma Physics, Office of Fusion Energy, Office of Energy Research, ER-542, Germantown, U.S. Department of Energy, Washington, DC 20545

94. K. Bol, Princeton Plasma Physics Laboratory, P.O. Box 451, Princeton, NJ 08544

95. R. A. E. Bolton, IREQ Hydro-Quebec Research Institute, 1800 Montee Ste.-Julie, Varennes, P.Q. JOL 2PO, Canada

96. D. H. Crandall, Experimental Plasma Research Branch, Division of Applied Plasma Physics, Office of Fusion Energy, Office of Energy Research, ER-542, Germantown, U.S. Department of Energy, Washington, DC 20545

97. R. L. Freeman, GA Technologies, Inc., P.O. Box 81608, San Diego, CA 92138

98. K. W. Gentle, RLM 11.222, Institute for Fusion Studies, University of Texas, Austin, TX 78712

99. R. J. Goldston, Princeton Plasma Physics Laboratory, P.O. Box 451, Princeton, NJ 08544

100. J. C. Hosea, Princeton Plasma Physics Laboratory, P.O. Box 451, Princeton, NJ 08544

101. S. W. Luke, Division of Confinement Systems, Office of Fusion Energy, Office of Energy Research, ER-55, Germantown, U.S. Department of Energy, Washington, DC 20545

102. E. Oktay, Division of Confinement Systems, Office of Fusion Energy, Office of Energy Research, ER-55, Germantown, U.S. Department of Energy, Washington, DC 20545

103. D. Overskei, GA Technologies, Inc., P.O. Box 81608, San Diego, CA 92138

104. R. R. Parker, Plasma Fusion Center, 167 Albany Street, Cambridge, MA 02139

105. W. L. Sadowski, Fusion Theory and Computer Services Branch, Division of Applied Plasma Physics, Office of Fusion Energy, Office of Energy Research, ER-541, Germantown, U.S. Department of Energy, Washington, DC 20545

106. J. W. Willis, Division of Confinement Systems, Office of Fusion Energy, Office of Energy Research, ER-55, Germantown, U.S. Department of Energy, Washington, DC 20545

107. A. P. Navarro, Division de Fusion, Junta de Energia Nuclear, Avenida Complutense 22, Madrid (3), Spain

108. Laboratory for Plasma and Fusion Studies, Department of Nuclear Engineering, Seoul National University, Shinrim-dong, Gwanak-ku, Seoul 151, Korea

109. L. M. Kovrizhnykh, Institute of General Physics, U.S.S.R. Academy of Sciences, Ulitsa Vavilova 38, 117924 Moscow, U.S.S.R.

110. O. Motojima, Plasma Physics Laboratory, Kyoto University, Gokasho, Uji, Kyoto, Japan

111. H. Wobig, Max-Planck Institut fur Plasmaphysik, D-8046 Garching, Federal Republic of Germany

112. J. L. Johnson, Plasma Physics Laboratory, Princeton University, P.O. Box 451, Princeton, NJ 08544

113. V. D. Shafranov, I. V. Kurchatov Institute of Atomic Energy, P.O. Box 3402, 123182 Moscow, U.S.S.R.

114. J. L. Shohet, Torsatron/Stellarator Laboratory, University of Wisconsin, Madison, WI 53706

115-222. Given distribution as shown in TIC-4500, Magnetic Fusion Energy (Category distribution UC-20)